Temporal Changes in the Areal Coverage of Daily Extreme Precipitation in the Northeastern United States Using High-Resolution Gridded Data

ARTHUR T. DEGAETANO, GRIFFIN MOOERS, AND THOMAS FAVATA

Northeast Regional Climate Center, Department of Earth and Atmospheric Science, Cornell University, Ithaca, New York

(Manuscript received 30 August 2019, in final form 11 December 2019)

ABSTRACT

Time-dependent changes in extreme precipitation occurrence across the northeastern United States are evaluated in terms of areal extent. Using gridded precipitation data for the period from 1950 to 2018, polygons are defined that are based on isohyets corresponding to extreme daily precipitation accumulations. Across the region, areal precipitation is characterized on the basis of the annual and seasonal number of extreme precipitation polygons and the area of the polygons. Using the subset of grid points that correspond to station locations in the northeastern United States, gridded precipitation replicates the observed trends in extreme precipitation based on station observations. Although the number of extreme precipitation polygons does not change significantly through time, there is a marked increase in the area covered by the polygons. The median annual polygon area nearly doubles from 1950 to 2013. Consistent results occur for percentiles other than the median and a range of extreme precipitation amount thresholds, with the most pronounced changes observed in spring and summer. Like trends in station data, outside the northeastern United States trends in extreme precipitation polygon area are negative, particularly in the western United States, or they are not statistically significant. Collectively, the results suggest that the increases in heavy precipitation frequency and amount observed at stations in the northeastern United States are a manifestation of an expansion of the spatial area over which extreme precipitation occurs rather than a change in the number of unique extreme precipitation polygons.

1. Introduction

Increases in extreme and total precipitation across regions of the United States and the country as a whole have been well documented in the literature (e.g., Kunkel et al. 2013a; Peterson et al. 2013; Hayhoe et al. 2007). The northeastern United States (Northeast), however, stands out as the region of the United States in which changes in extreme precipitation have been the most pronounced. The iconic Wuebbles et al. (2017) figure shows a 55% change in 99th-percentile precipitation and a 92% change in 5-yr-annual-recurrence 2-day precipitation events during the 1958–2016 period. The figure also illustrates the contrast in extreme precipitation trends between the eastern and western United States, with little significant change in extreme precipitation noted over the West Coast (Mass et al. 2011).

Typically, these studies have relied on station observations from the Global Historical Climatology Network (GHCN; Menne et al. 2012). In terms of total annual precipitation, Hayhoe et al. (2007) found a 10 mm decade^{-1} increase through the twentieth century. This matched Kunkel et al. (2013b), who, using climate division data, found an increase in total annual precipitation of 10.2 mm decade^{-1} from 1895 to 2011, as well as Keim et al. (2005), Mauget (2006), and, for New York, Rosenzweig et al. (2011). However, Huang et al. (2017) report a somewhat lower, but still significant, linear trend of 6.0 mm decade^{-1} based on GHCN data for the period 1901–2014.

In terms of extreme precipitation, changes in both frequency and intensity have been reported (e.g., Kunkel et al. 2013a; Pryor et al. 2009; DeGaetano 2009; Lai and Dzombak 2019; Armal et al. 2018). On a national basis, station-based extreme precipitation defined based on 2-day totals exceeding the 20% annual recurrence probability are most pronounced in the

Supplemental information related to this paper is available at the Journals Online website: https://doi.org/10.1175/JAMC-D-19-0210.s1.

Corresponding author: Art DeGaetano, atd2@cornell.edu

DOI: 10.1175/JAMC-D-19-0210.1

northeastern United States, where the number of events in the most recent decade are the largest since 1895 when the record began (Kunkel et al. 2013a). The trend in accumulated precipitation from daily events exceeding the 99th percentile is most significant in the Northeast for the period from 1957 to 2010, and it is also significant in the midwestern and southeastern United States (Kunkel et al. 2013a). Conversely, significant extreme precipitation trends are absent in the western United States.

On the global scale, changes in extreme precipitation have been linked to the human-caused increase in atmospheric greenhouse gases (e.g., Min et al. 2011) with a connection to increases in atmospheric water vapor. Kunkel et al. (2013a) observe that there has been a significant increase in atmospheric moisture associated with extreme precipitation events, especially over eastern parts of the United States. However, other mechanisms also control extreme precipitation occurrence.

Hoerling et al. (2016) argue that, over the southern United States, changes in precipitation extremes have been driven by teleconnections linked to eastern Pacific sea surface temperatures, but they could not ascribe a definitive large-scale cause to the changes observed in the Northeast. On the synoptic scale, Kunkel et al. (2012) found that a majority of the 20%-recurrence-interval events were associated with extratropical storm systems. Barlow (2011) showed that hurricanes contributed to the wettest days, but other studies (e.g., Groisman et al. 2012) do not find a link between increased precipitation extremes and tropical cyclones. Prein et al. (2017) point to changes in organized convective storms as a mechanism for increased future extreme precipitation.

A commonality of the studies cited above is the use of station-based precipitation records. Few studies have explored the use of gridded precipitation datasets to examine trends in precipitation extremes at locations other than those represented by GHCN stations. Huang et al. (2017) compared GHCN station data with a gridded station data product (Livneh et al. 2013) and North American Regional Reanalysis (NARR) output (Mesinger et al. 2006). They found that the Livneh data replicated regionally averaged annual and seasonal total station precipitation well (typically within 3%) and also captured the observed trends and a 2002 changepoint detected in the station data. NARR, on the other hand, underestimated total and seasonal precipitation by as much as 10% and was unable to capture the trends found in the station data.

Huang et al. (2017) defined extreme precipitation as that exceeding the 99th percentile of nonzero precipitation amounts. Annual (seasonal) extreme precipitation was then calculated as the sum of daily precipitation exceeding the threshold. Using this metric, they found that although the Livneh dataset was able to satisfactorily reproduce the seasonality and magnitude of extreme precipitation, it did not capture the trends or replicate a mid-1990s changepoint. The NARR data also underestimated extreme precipitation and did not give trends that were consistent with the observations.

A few studies have examined changes in the spatial extent of extreme rainfall. Wasko et al. (2016) used gauge data and found a reduction in the area of most intense precipitation at the storm scale. Chang et al. (2016) reached a similar conclusion using model output and radar data, while Dwyer and O'Gorman (2017) found mixed results when assessing changes in the zonal length of storm precipitation in model simulations.

There is an apparent dearth of studies that have examined changes in the spatial extent of extreme precipitation from a long-term climatological perspective. In this study we address this gap using analyses based on three gridded in situ precipitation datasets and a fourth satellite-estimated precipitation product. Rather than examining precipitation trends at individual grid points, spatially coherent polygons enclosing multiple grid points experiencing precipitation above a specific extreme threshold are identified. Time series of the number and area of these polygons are then assessed for time-dependent trends.

In section 2, the datasets are described. Section 3 discusses the methods that were employed with emphasis on the identification of extreme precipitation polygons (EPP) and assessment of the influence of the inherent data inhomogeneities. Results, which are focused on the northeastern United States given the pronounced trend in extreme rainfall frequency in this region (Wuebbles et al. 2017), are outlined in section 4. In addition, the analysis is extended to other regions of the United States, albeit in less detail, for comparison. Section 5 provides a summary and some concluding thoughts.

2. Data

Four gridded daily precipitation datasets are analyzed. The attributes of these datasets are summarized in Table 1 and briefly discussed in this section. Inconsistencies in the spatial density and distribution of station observations (e.g., Henn et al. 2018) and inherent biases in estimates of precipitation (especially extreme precipitation) from satellite-derived observations (e.g., Ombadi et al. 2018) present challenges in the use of these data in trend analysis. Using multiple datasets, derived using different methodologies and data sources,

TABLE 1. Summary of gridded datasets analyzed.

Dataset	Period of record	Resolution	Primary data	Reference
$NRCC_{NN}$	1950–present	4 km	GHCND[a]	—
L15	1950–2013	7 km	GHCND	Livneh et al. (2015)
PRISM	1981–present	4 km	GHCND	Daly et al. (2008)
PERSIANN	1983–present	25 km	ISCCP[b]	Ashouri et al. (2015)

[a] Global Historical Climatology Network Daily (Menne et al. 2012).
[b] International Satellite Cloud Climatology Project (Knapp 2008).

helps to illustrate the sensitivity of the results to data inhomogeneities and grid resolution and provides justification for ultimately selecting two datasets that minimize these biases.

a. NRCC interpolated station data

The Northeast Regional Climate Center (NRCC) natural neighbor–interpolated station data ($NRCC_{NN}$) has the longest temporal coverage of the datasets, extending from 1950 to the present, and is available from the Applied Climate Information System (ACIS; DeGaetano et al. 2015). In $NRCC_{NN}$, GHCN stations (Menne et al. 2012) reporting a 0500–0900 local standard time observation are interpolated to a 2.5-min grid (approximately 4 km × 4 km) using the natural-neighbor method. The preponderance of daily precipitation observations during this period follow a morning observation schedule, and therefore only this subset is used to avoid mixing daily precipitation accumulations from different time intervals. The total number of stations used in the interpolation varies daily, depending upon whether a given station reported (Fig. S1 in the online supplemental material). Nonetheless, over the period from 1950 to 2018, there has not been a systematic change in the number of available stations (Fig. 1). Over the 69-yr period, the number of available stations in the Northeast varied between 550 and 750 with few exceptions. The dataset is national in scope and is updated routinely to reflect the highest quality data in the GHCN.

b. PRISM

The Parameter–Elevation Regressions on Independent Slope Model (PRISM; Daly et al. 2008) is also used to define precipitation areas. Like $NRCC_{NN}$, the base data in the PRISM grid are obtained from the GHCN. Unlike $NRCC_{NN}$, topography is a key interpolation factor in PRISM (Daly et al. 2008). Precipitation observations are weighted based on topographic factors such as coastal proximity, slope, elevation, and aspect. Stations are grouped into facets and for each facet a regression function between precipitation and the topographic predictors is developed and then applied to a 30 arc s digital elevation grid (Daly et al. 2008).

Climatologically aided interpolation (CAI) is applied to the original surface station precipitation data used by PRISM (Daly et al. 2017). CAI draws on the long-term precipitation climatology to help define the spatial pattern of precipitation on a given day (Hunter and Meentemeyer 2005). PRISM assumes that the best-first approximation of the spatial pattern of precipitation for a given day is the pattern of long-term (1981–2010) precipitation. The interpolated precipitation values are subsequently smoothed based on an inverse distance weighting of pixels within 8 km of the point of interest (Daly et al. 2008). The final daily PRISM precipitation grid has a resolution of 2.5 min × 2.5 min, which is approximately 4 km × 4 km over the Northeast (PRISM Climate Group 2016).

After 2002, 4-km radar-based precipitation estimates have been used as a part of the PRISM interpolation in addition to station data (PRISM Climate Group 2016). The inclusion of radar data, the addition of data from networks other than the GHCN, and the lack of a consistent observation time for input data introduce discontinuities to time series of extreme precipitation events. For example, when ignoring observation time

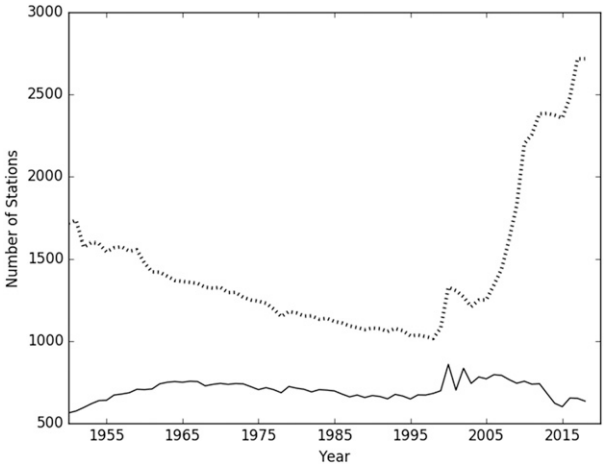

FIG. 1. Number of available GHCN precipitation stations to compute the daily $NRCC_{NN}$ (solid line) grid that requires a morning observation time and the PRISM (dotted line) grid that does not restrict observation time.

the number of available stations in GHCN increases dramatically in the early 2000s (Fig. 1). This is in part due to the inclusion of stations from the Community Collaborative Rain, Hail and Snow Network (CoCoRaHS), for which time-of-observation metadata are not included in GHCN. The increased spatial detail afforded by the radar data, results in an increase in the number of unique extreme precipitation areas. This is particularly the case for smaller ($<1000\,km^2$) areas. Therefore, analyses using PRISM were limited.

c. *Livneh et al. data*

The Livneh et al. (2013, 2015) dataset (hereinafter the "L15" dataset) is based on daily observing stations from the NOAA Cooperative Observer Network included in the GHCN. The data cover the period from 1950 to 2013. Precipitation data are interpolated to a 0.0625° grid (approximately 7 km in the Northeast) using the methods of Shepard (1984) and Widmann and Bretherton (2000) consistent with the method used by Maurer et al. (2002). Here station-specific precipitation ratios (relative to the 30-yr average) are interpolated to a grid using a weighted average based on distance and directionality (to avoid overweighting a cluster of stations relative to an isolated station located in a different sector). Daily interpolated values are further scaled to assure that the accumulation of daily precipitation amounts match the long-term monthly average PRISM climatology. This long-term PRISM climatology is based on a consistent set of stations that are free of the biases discussed previously. In the L15 method, the recorded time of observation is used to apportion daily precipitation totals to a common calendar day prior to interpolation.

d. *PERSIANN climate data record*

The Precipitation Estimation from Remotely Sensed Information Using Artificial Neural Networks Climate Data Record (PERSIANN-CDR) is derived from gridded satellite infrared data (GridSat-B1) and adjusted by the Global Precipitation Climatology Project (GPCP) (Ashouri et al. 2015). International Satellite Cloud Climatology Project (ISCCP) IR brightness temperature data using infrared wavelengths between 10.0 and 12.0 μm from geostationary satellite sources serve as input to the PERSIANN algorithm (Ashouri et al. 2015; Sorooshian et al. 2000). Using an artificial neural network, the algorithm identifies cold cloud pixels and associates variations in brightness temperature to surface precipitation rate. The PERSIANN algorithm is pretrained using Stage IV hourly precipitation data (Ashouri et al. 2015). The data are processed to a 25 km × 25 km resolution.

PERSIANN data undergo bias correction using the GPCP (Adler et al. 2003). The GPCP combines data from 27 different sources, both precipitation data from rain gauges and satellite-estimated precipitation data, to get a blended precipitation dataset (Adler et al. 2003).

3. Methods

a. *Computation of precipitation areas*

For each gridded dataset, areas of precipitation exceeding a specified extreme daily precipitation total were identified. A threshold of 5.08 cm was chosen on the basis of its use to define extreme rainfall in foundational papers describing trends (e.g., Easterling et al. 2000), to align with one of the core climate change indices (ETCCDI 2013) and in the Northeast to correspond to the one-in-5-yr-occurrence event analyzed in recent studies (e.g., Kunkel et al. 2013a). A fixed threshold amount is used, as opposed to one based on a fixed percentile, to avoid subdividing areas of cohesive precipitation amounts based on grid-to-grid differences in climatological percentiles.

Given the daily resolution of the gridded datasets, EPP do not necessarily represent the total precipitation from a specific weather event but characterize the spatial pattern of rainfall on a given calendar day. For each daily precipitation grid, a five-step method was used to define EPPs and compute each polygon's area.

(i) The first step is to *identify EPP.* The matplotlib software pyplot library contour function uses a marching-squares approach to develop a set of isolines corresponding to a specified extreme precipitation value (e.g., 5.08 cm) given a two-dimensional data array (in this case the daily precipitation grid). A schematic visualization of the marching-squares method is given online (https://en.wikipedia.org/wiki/Marching_squares).

(ii) The second step is to *extract line segments defining polygons.* The matplotlib software get_paths module is used to find a set of closed line segments that defines the extreme precipitation polygons associated with each day.

(iii) The third step is to *convert line segments to convex hulls.* The scipy.spatial software ConvexHull class uses the "quickhull" algorithm of Barber et al. (1996). The resulting convex hulls facilitate the computation of EPP area and are indistinguishable from the matplotlib contour paths obtained in step i.

(iv) The fourth step is to *modify convex hulls* using the matplotlib software path.contains_path() function and the scipy.spatial.distance, pyproj software transform

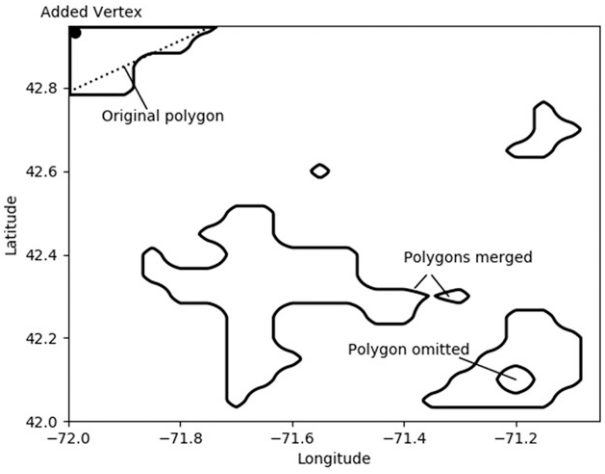

FIG. 2. Illustration of cases that required modification of the specified convex hulls. Contours depict extreme precipitation contours.

function. There are three situations in which the polygons described by the convex hulls are modified (as illustrated in Fig. 2):

1) In situations where the endpoints of a polygon bracket the corner of the domain boundary, a vertex is added at the corner. Without such a point, the convex hull often omitted the area in the corner of the domain (Fig. 2).
2) It is also possible for two or more polygons to be nested within each other, as in the lower-right corner of Fig. 2. This occurs when there are grid points with precipitation that is less than the threshold within a more extensive area of greater-than-threshold precipitation. These interior polygons (enclosing the areas of less-than-threshold precipitation) are identified using the path.contains_path() function and ultimately excluded.
3) Given the spatial resolution of the gridded precipitation data, it was also possible that the contouring algorithm divided an otherwise coherent area into multiple distinct polygons. To avoid this, a minimum separation distance threshold was implemented. Individual extreme precipitation areas that were separated by a distance of less than this threshold were combined. Two distances (10 and 100 km) were used to test the sensitivity of this parameter. The scipy.spatial.distance algorithm was used to identify the closest convex hull boundaries, and the pyproj library (https://pypi.org/project/pyproj/) was used to convert the map coordinates to geometric distance. Since the choice of separation distance had little effect on the results, only the 100-km threshold is used.
(v) The fifth and final step is to *compute EPP area*, using the pypi.org project software area function. In this final step, the area enclosed by each modified polygon is converted from coordinate space to geometric area.

b. Statistical analysis

Theil slopes were used to determine time-dependent trends in both the number and area of the extreme precipitation polygons. The significance of the identified slopes was quantified based on the Kendall's tau correlation coefficient test. Three classes of time series were examined. First, to ascertain whether the gridded datasets reflected the documented trends in extreme precipitation using the station record, grid points corresponding to GHCN station locations were selected. Stations were limited to those with <10% of the potentially available daily observations missing during the 1950–2018 time period. A total of 356 stations met this criterion (online supplemental Fig. S1). For both the closest grid point and the station itself, the annual and seasonal number of occurrences exceeding the extreme threshold were tallied. Then the numbers of occurrences in a given year were summed across all stations in a region and divided by the number of stations to get an annual mean value.

The gridded data were also randomly sampled to assess whether the gridpoint trends were an artifact of the location of the stations. In each of 1000 replications, 356 grid points were randomly selected, a regional average computed, and trends calculated. The resulting trends were then compared with those representing the station locations.

The other two classes of time series were based on the set of extreme precipitation polygons. First, the total number of unique extreme precipitation polygons, regardless of size, was tallied for each year and season and the associated trends assessed. Then polygon area was considered by developing annual and seasonal series of regional 10th-, 25th-, 50th-, and 75th-percentile and maximum polygon area.

4. Results

Three broad categories of results are discussed. In section 4a, the ability of the gridded datasets to replicate the station-based trends documented in previous studies is evaluated. Select gridpoint values are used to simulate station data and comparisons among the datasets conducted based on this metric. In sections 4b and 4c,

TABLE 2. Periods of record, means, and standard deviations of annual 5.08-cm daily precipitation counts based on station observations and four gridded datasets.

Grid name	Period of record	Mean	Std dev
Station	1981–2013	1.47	0.46
$NRCC_{NN}$	1981–2013	1.20	0.46
PRISM	1981–2013	1.28	0.32
L15	1981–2013	0.48	0.29
PERSIANN	1983–2018	0.39	0.25

time-dependent trends in EPP counts and areas are presented and inconsistencies related to the PRISM and PERSIANN datasets are discussed. In sections 4d–4f, EPP trends based on the $NRCC_{NN}$ and L15 datasets are assessed from a seasonal prospective and with regard to the sensitivity of the choice of extreme precipitation amount threshold. The Northeast-specific results are also compared with the other National Climate Assessment (NCA) regions within the continental United States.

a. Single grid point

The average regional number of 5.08-cm daily precipitation events is similar in the station, $NRCC_{NN}$, and PRISM datasets. Over the common 1981–2013 period, averaged across the Northeast, station counts are slightly higher than the average annual counts associated with the PRISM and $NRCC_{NN}$ gridpoint values (Table 2). The annual counts are lower using the L15 dataset (Table 2) with even fewer counts based on the PERSIANN grid. The interannual variance also varies with dataset. The higher spatial resolution $NRCC_{NN}$ and PRISM data exhibit standard deviations that are in line with the station data (Table 2). Lower variance occurs in the coarser-resolution data grids. Although resolution is one of the differentiating features of the datasets, it is not the only factor that leads to these differences. Timmermans et al. (2019) point to source data as a primary segregation mechanism and demonstrate that satellite-based products tend to show smoother spatial features, especially PERSIANN.

Despite these differences, except for PERSIANN, the trends in the occurrence of one-day 5.08-cm precipitation events were similar among the datasets (Fig. 3). Regardless of the period of record or dataset, the trends were consistently positive and statistically significant at the two-tailed 95% level. Over the period from 1950 to 2013, 5.08-cm precipitation occurrences increased by 34%–43% (0.003–0.009 events per year) depending on dataset. The station observations and L15 values had the

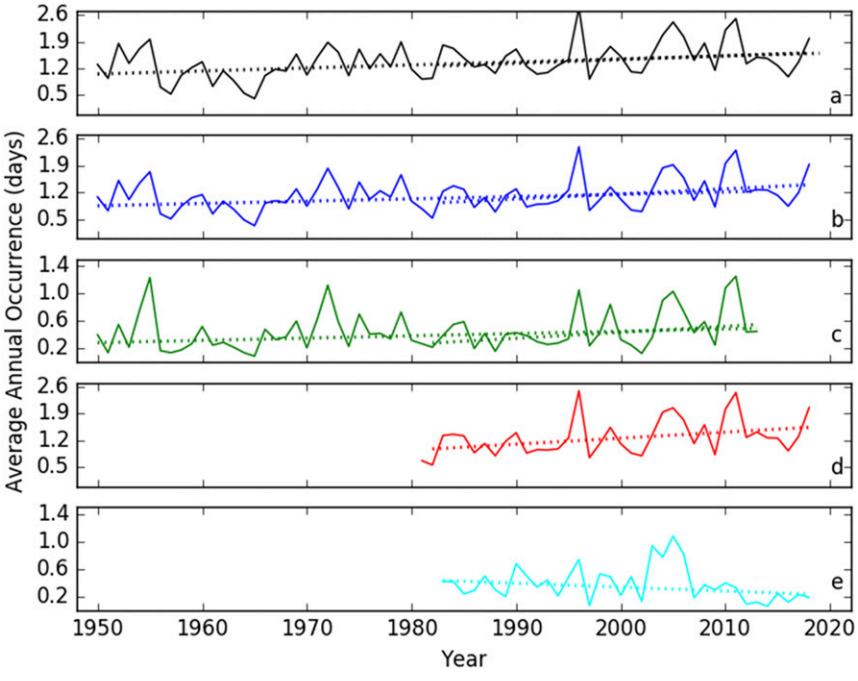

FIG. 3. Time series of average annual counts of point precipitation exceeding 5.08 cm in the Northeast for (a) station locations and (b) $NRCC_{NN}$, (c) L15, (d) PRISM, and (e) PERSIANN grid points corresponding to station locations. Theil slopes corresponding to each dataset's period of record are shown by dashed lines. In (a)–(c), the second dashed line depicts the slope over a period of record that is in common with that of the PERSIANN data.

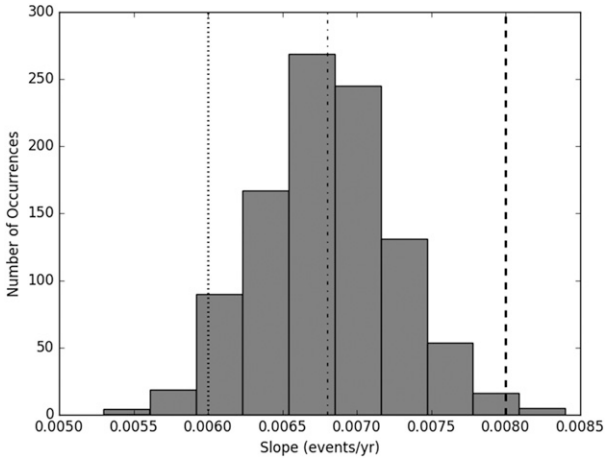

FIG. 4. Histogram of extreme precipitation event time series slopes from 1000 randomly selected 356-gridpoint networks from the Northeast. The vertical lines correspond to the time series slope identified for the station data (dashed) and the network of $NRCC_{NN}$ grid points associated with the stations (dotted) and the mean of the random $NRCC_{NN}$ gridpoint slopes (dot–dashed).

greatest percent increase (43% and 42%, respectively) in this period. These results are unaffected when a higher missing data threshold (20% vs 10%) was implemented.

For the shorter 1981–2013 period, the trends in the station, $NRCC_{NN}$ and L15 datasets (Figs. 3a–c) were again similar and the rate of change tended to be greater (0.009–0.018 events per year or between 1.2% yr^{-1} and 1.7% yr^{-1}). The PRISM (Fig. 3d) values also increase at a similar rate (0.021 event per year; 1.6% yr^{-1}). These rates of change are also generally consistent (despite differences in period of record and definition of extreme threshold) with those reported in the literature for station observations. For instance, in the Northeast, Hoerling et al. (2016) show a 6%–8% per decade increase in the frequency of very wet days from 1979 to 2013, with much of the increase coming in May–October.

The PERSIANN grid values behaved differently (Fig. 3e). Over its 1983–2018 period of record, 5.08-cm precipitation events declined at a statistically significant rate of −0.006 events per year (−1.4% yr^{-1}) averaged over the 356 grid points closest to the station locations. While it is not clear why PERSIANN exhibits this distinctive behavior, there is a propensity for satellite-based products to underestimate heavy precipitation (Ombadi et al. 2018).

Using the $NRCC_{NN}$ data grid, the frequency of slopes obtained from 1000 randomly sampled sets of 356 grid points is shown in Fig. 4. The slopes are largely consistent with those based on grids approximating the station locations. For the grid networks of random locations, the slopes tend to be greater than that for the network representing the station locations, but less than that of the station data. Thus, the majority of random-location slopes fall between $NRCC_{NN}$ and station observation slopes shown in Fig. 3. The slopes in all but six of the

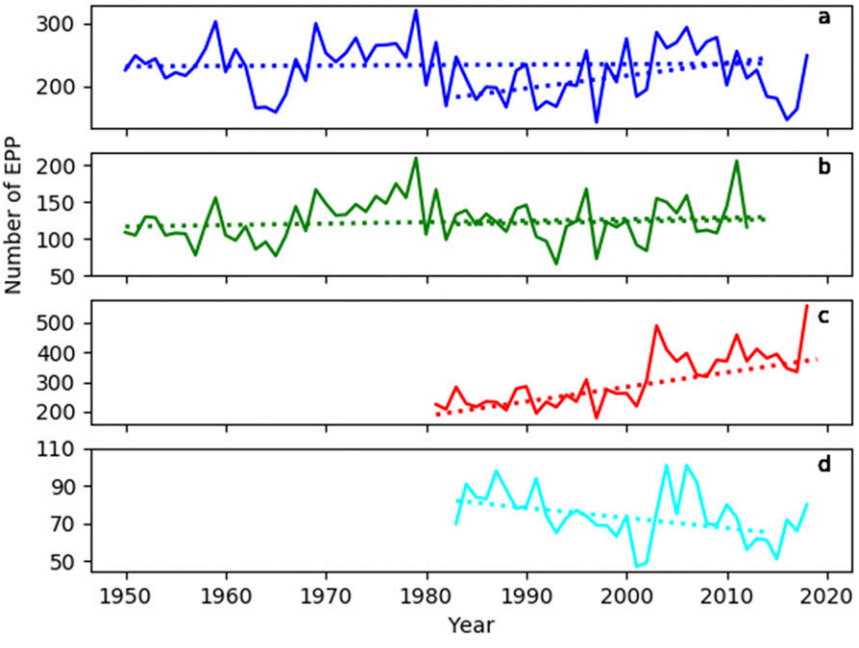

FIG. 5. Average annual number of 5.08-cm EPP polygons derived from (a) $NRCC_{NN}$, (b) L15, (c) PRISM, and (d) PERSIANN data. The dotted lines show the Theil slope for the period 1950–2013 or 1983–2013.

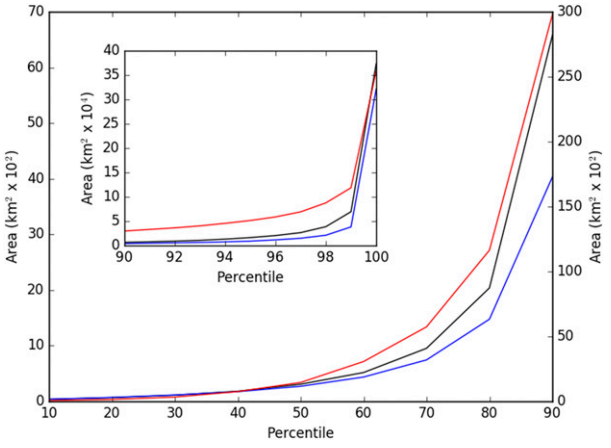

FIG. 6. Cumulative distribution functions of Northeast EPP areas (axes reversed to account for the difference in EPP areas between datasets) for $NRCC_{NN}$ (black), L15 (blue), and PERSIANN (red). PERSIANN areas are shown on the secondary y axis on the right. The inset shows the portions of the cumulative distribution functions that correspond to the 90th percentile–maximum area.

randomly selected networks of 356 grid points were significant at the $\alpha = 0.05$ level.

b. Number of areas

The increasing frequency of 5.08 cm precipitation events at station or individual gridpoint locations can arise from two features of the spatial distribution of extreme precipitation. Either the number of EPP can increase, or the area enclosed by EPPs can increase; both of these spatial features are intrinsically linked to changes in the intensity and/or duration of precipitation. Figure 5 shows that the number of EPP has remained constant across the Northeast, particularly since 1950 in two of the datasets. Using the L15 dataset (Fig. 5b) a gentle positive slope (0.2 EPP per year or approximately 0.2% per year) is observed in both the 1950–2013 ($p = 0.25$) and 1983–2013 ($p = 0.75$) periods. This is similar to the behavior of the $NRCC_{NN}$ time series in the 1950–2013 period, that shows an even less significant positive slope (Fig. 5a). The $NRCC_{NN}$ time series exhibits a significant increase in EPP counts in the 1983–2013 period, but this is likely an artifact of the choice of end years. For the 1983–2018 period, the $NRCC_{NN}$ slope becomes nonsignificant. The PRISM data show an abrupt increase in the number of EPP after 2002 (Fig. 5c). Since this stemmed from systematic temporal discontinuities related to the inclusion of radar data and a sharp increase in available GHCN stations (Fig. 1), the PRISM data were excluded from further analysis.

The coarser-resolution PERSIANN dataset, exhibits a different time-dependent behavior, with EPP counts declining at a significant rate of 0.5 EPP per year in both

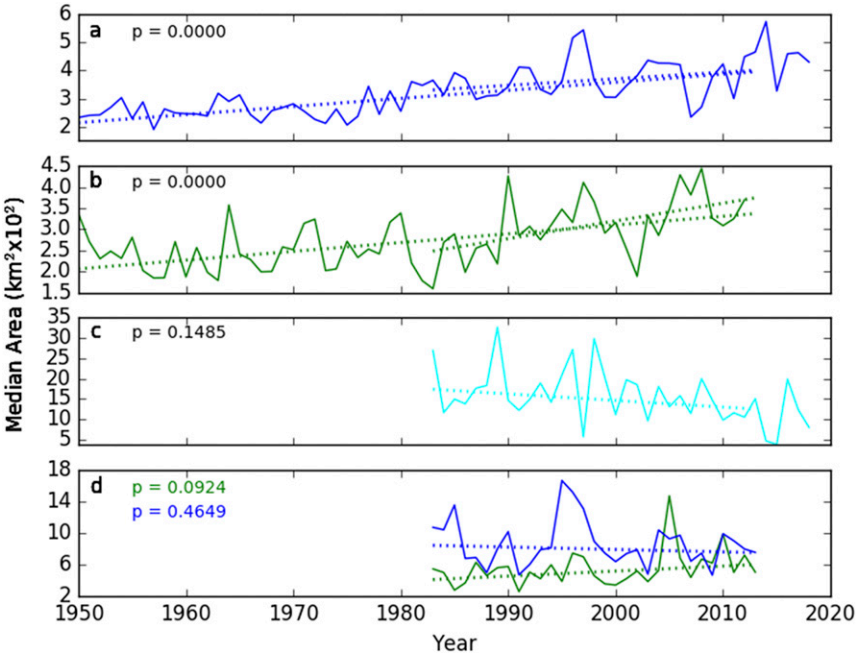

FIG. 7. Median annual total area encompassed by 5.08-cm EPP polygons derived from (a) $NRCC_{NN}$, (b) L15, and (c) PERSIANN data and (d) L15 (green) and $NRCC_{NN}$ (blue) regridded to the coarser PERSIANN resolution. The dotted lines show the Theil slope for the periods 1950–2013 or 1983–2013. The p value for the longest time period is indicated.

the 1983–2013 ($p = 0.03$) and 1983–2018 ($p = 0.01$) periods (Fig. 5d). The PERSIANN data also exhibited a trend that was opposite to those for daily 5.08-cm extreme precipitation occurrence in the station, $NRCC_{NN}$, L15, and PRISM data (Fig. 3).

c. Size of areas

The empirical probability distribution of areas enclosed by the EPPs is highly right skewed. On the basis of the cumulative distribution function shown in Fig. 6, the lowest 50% of the $NRCC_{NN}$ and L15 EPP areas encompass a similar range of values from 16 to 300 km^2. For larger EPPs, the 75th-percentile areas are 30% larger in the $NRCC_{NN}$ data (1350 vs 1000 km^2). At the 90th percentile, the $NRCC_{NN}$ EPP area is 60% larger than the L15 value (6777 vs 4031 km^2). The maximum EPP areas are two orders of magnitude larger than the 90th percentile, but the areas are more similar among the datasets, varying by 16% (3.7×10^5 vs 3.2×10^5 km^2).

PERSIANN EPP areas are consistently larger than those for $NRCC_{NN}$ and L15. Both the median and 90th-percentile areas are 4–7 times as large as that given by the $NRCC_{NN}$ and L15 values. Despite this, the most extreme PERSIANN EPP area (3.6×10^5 km^2) is similar to that given by the other grids. This is an indication that coarser PERSIANN grids are able to characterize regional-scale extreme precipitation events as well as the finer-resolution grids but overly smooth smaller-scale extreme precipitation areas. For perspective, an area of 3.6×10^5 km^2 would cover New York, Pennsylvania, New Jersey, and the three southern New England states. An example of an event with this spatial scale occurred on 1 October 2010 when an upper-level low pressure system interacted with moisture from Tropical Storm Nicole.

The median EPP areas have significantly increased through time on the basis of both the $NRCC_{NN}$ (Fig. 7a) and L15 (Fig. 7b) data. The trends are consistent over the 1950–2013 period, which is common to both datasets. The median EPP area has increased by 2.8 $km^2\,yr^{-1}$ in the $NRCC_{NN}$ data and 2.1 $km^2\,yr^{-1}$ in L15. For a more recent period, 1983–2013, chosen because of its overlap with the PERSIANN data record, the $NRCC_{NN}$ slope is similar (2.3 $km^2\,yr^{-1}$) while the L15 slope is steeper (4.2 $km^2\,yr^{-1}$). This larger slope is partially an artifact of 1983 corresponding to the minimum of the L15 time series as the slope for the 1984–2013 and 1985–2013 periods is less (3.4 $km^2\,yr^{-1}$).

The PERSIANN data series does not exhibit the same time-dependent behavior (Fig. 7c). Instead EPP decreases, but at a rate that is not statistically significant. To examine whether the coarser resolution of the PERSIANN precipitation was responsible for this difference, the L15 and $NRCC_{NN}$ datasets were upscaled to the PERSIANN resolution using the bilinear interpolation function from the matplotlib basemap toolkit (https://matplotlib.org/basemap/api/basemap_api.html). Although the trend in median EPP area from the coarsened L15 data remained positive (Fig. 7d), the trend's significance fell from $p = 0.01$ at the original resolution to $p = 0.09$. The $NRCC_{NN}$ trend also changed, reversing from significantly positive to negative (Fig. 7d). Timmermans et al. (2019) urge caution in the use of gridded satellite precipitation in extreme analyses because of difficulties resolving precipitation over complex terrain, generally coarser resolution than rain gauge–based interpolations, and the nondirect measurement of precipitation from radiation measurements. Likewise, Nguyen et al. (2018) document that PERSIANN underestimates extreme rainfall in the continental United States. Thus, subsequent analyses are based only on the $NRCC_{NN}$ and L15 data.

TABLE 3. Theil slopes[a] associated with seasonal changes in 5.08-cm precipitation occurrence at single points (events per year), EPP counts (polygons per year), and annual median EPP area ($km^2\,yr^{-1}$). Significant ($p < 0.05$) slopes are shown in boldface type.

Dataset	Winter	Spring	Summer	Autumn
Single point				
Station	**0.002**	**0.003**	**0.003**	0.003
$NRCC_{NN}$	0.001	**0.002**	0.001	0.002
L15	0.000	**0.001**	0.001	0.001
EPP count				
$NRCC_{NN}$	0.000	0.066	**−0.362**	−0.037
L15	0.000	**0.167**	−0.035	−0.551
EPP area				
$NRCC_{NN}$	**2.58**	**4.66**	**2.61**	1.77
L15	0.33	**2.58**	**2.07**	0.93

[a] Slopes are computed on the basis of the 1950–2018 period of record, except for L15, which ends in 2013.

d. Seasonal trends

From a seasonal perspective, Table 3 shows that trends in Northeast EPP median area are significant and greatest in during spring and summer. Neither the $NRCC_{NN}$ nor L15 dataset indicates a significant trend in autumn EPP median area. Consistent with the annual results, trends in seasonal EPP counts are generally not significant and in some cases decreasing (annual EPP counts decline slightly with time in the $NRCC_{NN}$ data). At point locations corresponding to station locations, both gridded datasets show significant positive trends in extreme precipitation counts during spring and nonsignificant positive trends during fall, in agreement with the station data. Trends are also

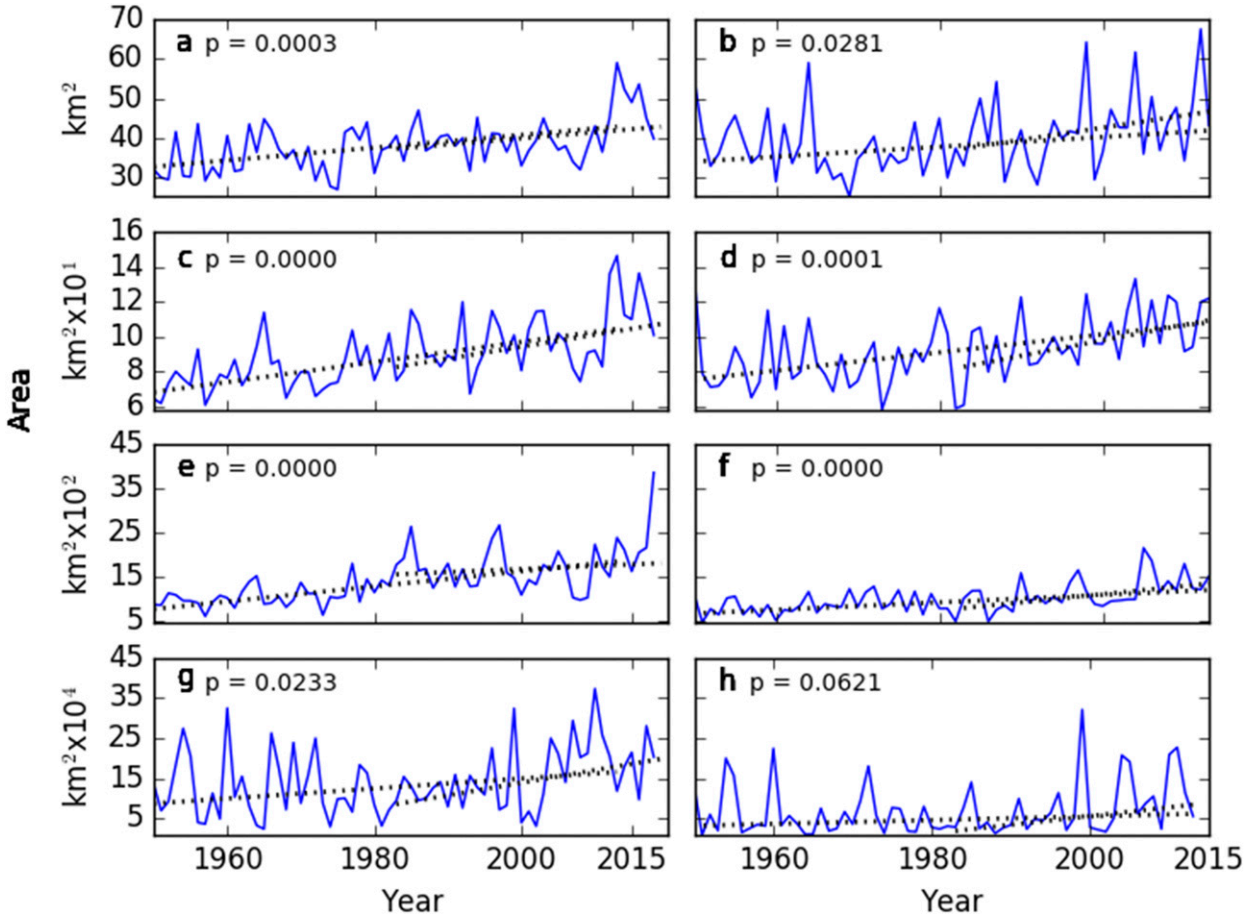

FIG. 8. Annual (left) $NRCC_{NN}$ and (right) L15 (a),(b) 10th-, (c),(d) 25th-, (e),(f) 75th-percentile, and (g),(h) maximum area encompassed by 5.08-cm EPP polygons. The dotted lines show the Theil slope for the period 1950–2013 or 1983–2013. The p value for the 1950–2013 period is also indicated.

positive based on each of the three datasets in summer and winter, but only the station trends are statistically significant.

e. Sensitivity to percentile and precipitation thresholds

Trends in Northeast EPP area percentiles other than the median are consistent (Fig. 8). In all cases the trend in the annual 10th-, 25th-, and 75th-percentile area (Figs. 8a–f) is positive and statistically significant ($p < 0.03$). There is not a consistent relationship between slope and percentile. Like the median, the trends in the 1950–2013 period are similar to those computed over the 1983–2013 period. In the L15 data, however, there is a tendency for the slope to be greater in the shorter (more recent) time period. The maximum annual EPP area also increased in both datasets (Figs. 8g,h). Only the maximum annual EPP area trend for the L15 data did not attain significance at the $\alpha = 0.05$ level ($p = 0.062$).

Northeast annual median EPP area trends defined using other extreme thresholds (2.54, 7.62, and 10.16 cm) also matched those based on the 5.08-cm threshold (Fig. 9). In all cases the trends are positive and, with the exception of the 10.16-cm threshold, are statistically significant. The trends for the 1983–2013 period also tend to be greater than those for the full record, as was the case with the 5.08-cm threshold. It is possible for the EPP median area for a higher precipitation threshold to exceed that based on a lower threshold. The distribution of areas based on lower thresholds are heavily right skewed as opposed to more uniform as is the case with higher thresholds.

f. Other regional trends

The significant median annual EPP area trends identified in the Northeast region, are not characteristic of other regions in the United States (Fig. 10). The L15 dataset is used given its similarity to the $NRCC_{NN}$ results in the Northeast and its consideration of the

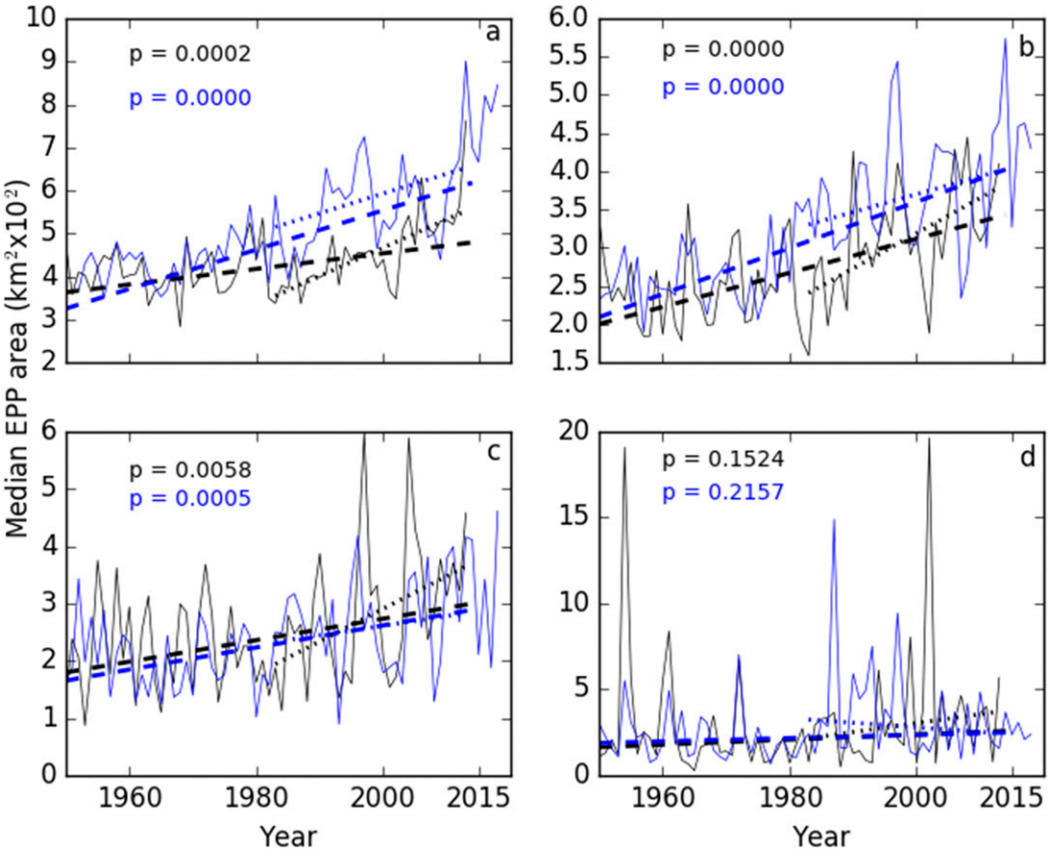

FIG. 9. Median annual total area encompassed by (a) 2.54-, (b) 5.08-, (c) 7.62-, and (d) 10.16-cm EPP polygons derived from $NRCC_{NN}$ (blue) and L15 (black). Also shown is the Theil slope for the period 1950–2013 (dashed lines) or 1983–2013 (dotted lines). The *p* values for the longest time period is indicated.

elevation gradients and sparser station density in more western regions. In adjacent regions, a statistically significant increase in median 5.08-cm EPP area occurs in the Southeast NCA region (Fig. 10a), but to the west in the Midwest NCA region, the increasing trend in EPP area is not significant (Fig. 10b). Trends in 2.58-cm EPP area are either nonsignificant or decreasing.

In the western United States, median annual EPP trends are significantly negative in both the Northwest and Southwest NCA regions, regardless of precipitation threshold. In the central part of the United States, the large Great Plains NCA region was divided into northern and southern subregions, with the southern Great Plains encompassing Kansas, Oklahoma, and Texas. In both subregions median annual EPP area decreases through time, with only that using the 2.54-cm threshold in northern Great Plains attaining statistical significance.

In all NCA regions outside the Northeast, EPP counts decrease with time (not shown). Significant decreases are noted in the Northwest, Southwest, and northern Great Plains regions. These areas showed the largest declines in EPP area.

5. Summary and conclusions

The significant increase in extreme daily precipitation occurrence at station locations in the northeastern United States that has been documented in previous studies appears to correspond to an increase in the spatial area that receives extreme precipitation on a given day. Using two datasets that interpolate station observations to a high-resolution (<10 km) grid and minimize temporal data inconsistencies, the following was found:

1) Trends in station-based extreme precipitation occurrence are replicated by grid points representing the station locations as well as random selections of *n* grid points, where *n* is the number of available stations.
2) There has been no significant or consistent change in the number of EPPs (individual polygons defined

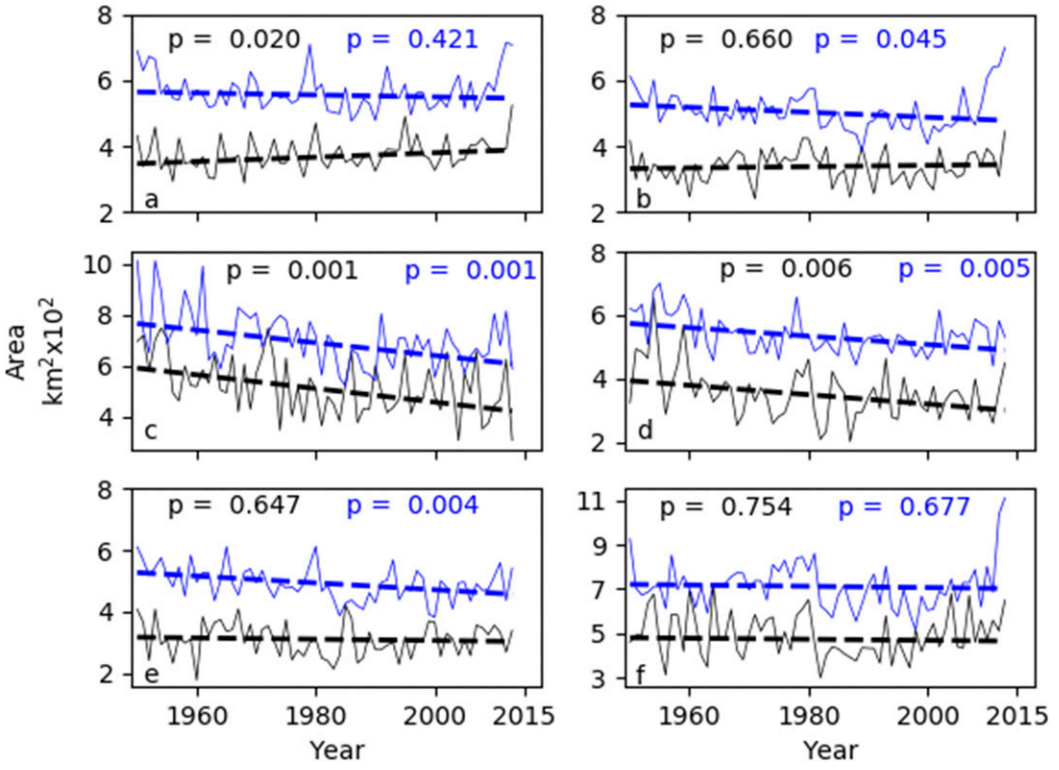

FIG. 10. Median annual total area encompassed by 5.08- (black) and 2.54-cm (blue) EPP polygons derived from L15 for the (a) Southeast, (b) Midwest, (c) Northwest, (d) Southwest, (e) northern Great Plains, and (f) southern Great Plains NCA regions. The dotted lines show the Theil slope for the period 1950–2013. The *p* value for each dataset's slope is also given.

by a specific extreme isohyet) that occur each year across the Northeast.

3) The annual median area of EPP has increased significantly at a rate of between 2 and 3 $km^2 yr^{-1}$ over the period from 1950 to 2013. This represents about a doubling of the annual median EPP areas common in 1950.
4) Similar increases are found in EPP areas corresponding to percentiles other than the median and extreme precipitation thresholds other than 5.08 cm.
5) On a seasonal basis, the increase in EPP area is most pronounced in the spring and summer. The $NRCC_{NN}$ grid also indicates a significant increase in EPP area in winter.
6) In regions outside the Northeast, where trends in station-based extreme precipitation are not as strong, trends in EPP area are generally not significant or decreasing. The Southeast, which saw a significant increase, is an exception.

Collectively, these findings suggest that the increases in station-based precipitation extremes reported in the literature for the Northeast result from a general expansion of the geographic area affected by extreme precipitation, rather than an increase in the number of EPP. This increase in geographic coverage occurs regardless of EPP size, as similar trends are detected across the EPP area distribution, and also regardless of the threshold used to define extreme. However, the change is tempered for the largest EPP (e.g., the annual maximum EPP area) and the most extreme thresholds (e.g., ≥10.16 cm). Such a finding is consistent with a general moistening of the atmosphere (e.g., Trenberth et al. 2018), in which, for example, a uniform increase in precipitation amounts across the precipitation shield would lead to a larger area of rainfall above a fixed threshold.

While the results are consistent with the many studies that have documented changes in the frequency and intensity of extreme rainfall at observing stations, they conceptually differ from those that have examined extreme rainfall at the individual storm scale. Both Wasko et al. (2016) and Chang et al. (2016) found a contraction of the area of most intense precipitation within a given storm. In model simulations, Dwyer and O'Gorman (2017) found that stronger winds increase storm speed and hence shorten the time period that any particular

location receives extreme rainfall. Examining how this translates to daily EPP area would provide a physical causal mechanism to our empirical results. Conceivably, faster-moving storms could spread extreme rainfall over a broader area, despite limiting rainfall at a specific point. As Dwyer and O'Gorman (2017) point out, changes in the size of the eddies that encompass the extreme precipitation could also impact EPP area.

In addition to providing new insight into a potential underlying mechanism for the increased extreme precipitation occurrence at Northeast stations, particularly vis-à-vis other regions of the United States that have experienced smaller increases in extreme precipitation, the results also have practical implications. For instance, a systematic change in the spatial extent of extreme precipitation would affect existing empirical relationships relating point precipitation observations to areal precipitation amounts (e.g., Le et al. 2018).

The increases are consistent between two different gridded datasets. Although both depend on the GHCN station observations, they differ in the subset of GHCN stations that is used and the method of spatial interpolation. In one case, daily precipitation is a simple natural neighbor interpolation among the station values, while in the other, a greater number of stations is used and the interpolations scaled to match the long-term PRISM climatology, which accounts for topographic and coastal influences (Livneh et al. 2013, 2015). Because both of these datasets also have a >60 year period of record, the influence of decadal variability on the trends is reduced. Although beyond the scope of this work, examining areal extreme precipitation extent as a function of different modes of large-scale climate variability is an interesting avenue for future research.

Examination of EPP area trends using two additional datasets with shorter periods of record highlight how differences in base data sources and grid resolution affect the resultant trends. In the case of PRISM, the incorporation of radar-estimated precipitation during the early 2000s greatly increased the number of EPP polygons. This created an artificial discontinuity in the EPP area time series as many more small areas were identified in the radar era. Conversely, the EPP area trend based on the coarser-resolution PERSIANN data grid was not significant and negative. Although Timmermans et al. (2019) and Chen et al. (2014) cite other causes, this difference appears to have been at least partially due to the base resolution of the PERSIANN grid. When the L15 and $NRCC_{NN}$ grids were upscaled to the PERSIANN resolution (a single 0.25° PERSIANN grid cell encompasses approximately 9 L15 and 36 $NRCC_{NN}$ grids), none of the annual percentile areas showed a significant increase with time (Fig. S2 in the online supplemental material). This is despite the presence of significant trends in 10th-, 25th-, 50th-, and 75th-percentile EPP area as based on the original-resolution L15 and $NRCC_{NN}$ grids. For maximum area, the trends in the upscaled values were more similar to those using the original L15 and $NRCC_{NN}$ grid resolution. This is not unexpected given the largest annual EPP polygon areas are similar among the datasets. These differences highlight the need for long-term gridded precipitation datasets that are free of methodological and base data discontinuities. Future datasets that employ the PRISM (or similar) radar-based interpolations over a longer record will be instrumental in subsequent evaluations of temporal EPP area changes.

Acknowledgments. This work was supported by NOAA Contract AB-133E-16-CQ-0025. The work is an extension of undergraduate research honors theses submitted by Mr. Mooers and Mr. Favata as students in the College of Agriculture and Life Sciences at Cornell University.

REFERENCES

Adler, R. F., and Coauthors, 2003: The Version-2 Global Precipitation Climatology Project (GPCP) monthly precipitation analysis (1979–present). *J. Hydrometeor.*, **4**, 1147–1167, https://doi.org/10.1175/1525-7541(2003)004<1147:TVGPCP>2.0.CO;2.

Armal, S., N. Devineni, and R. Khanbilvardi, 2018: Trends in extreme rainfall frequency in the contiguous United States: Attribution to climate change and climate variability modes. *J. Climate*, **31**, 369–385, https://doi.org/10.1175/JCLI-D-17-0106.1.

Ashouri, H., K. L. Hsu, S. Sorooshian, D. K. Braithwaite, K. R. Knapp, L. D. Cecil, B. R. Nelson, and O. P. Prat, 2015: PERSIANN-CDR: Daily precipitation climate data record from multisatellite observations for hydrological and climate studies. *Bull. Amer. Meteor. Soc.*, **96**, 69–83, https://doi.org/10.1175/BAMS-D-13-00068.1.

Barber, C. B., D. P. Dobkin, and H. Huhdanpaa, 1996: The quickhull algorithm for convex hulls. *ACM Trans. Math. Software*, **22**, 469–483, https://doi.org/10.1145/235815.235821.

Barlow, M., 2011: Influence of hurricane-related activity on North American extreme precipitation. *Geophys. Res. Lett.*, **38**, L04705, https://doi.org/10.1029/2010GL046258.

Chang, W., M. L. Stein, J. Wang, V. R. Kotamarthi, and E. J. Moyer, 2016: Changes in spatiotemporal precipitation patterns in changing climate conditions. *J. Climate*, **29**, 8355–8376, https://doi.org/10.1175/JCLI-D-15-0844.1.

Chen, S., and Coauthors, 2014: Evaluation of high-resolution precipitation estimates from satellites during July 2012 Beijing flood event using dense rain gauge observations. *PLOS ONE*, **9**, e89681, https://doi.org/10.1371/journal.pone.0089681.

Daly, C., M. Halbleib, J. I. Smith, W. P. Gibson, M. K. Doggett, G. H. Taylor, J. Curtis, and P. P. Pasteris, 2008: Physiographically sensitive mapping of climatological temperature and precipitation across the conterminous United States. *Int. J. Climatol.*, **28**, 2031–2064, https://doi.org/10.1002/joc.1688.

——, M. E. Slater, J. A. Roberti, S. H. Laseter, and L. W. Swift Jr., 2017: High-resolution precipitation mapping in a mountainous

watershed: Ground truth for evaluating uncertainty in a national precipitation dataset. *Int. J. Climatol.*, **37**, 124–137, https://doi.org/10.1002/joc.4986.

DeGaetano, A. T., 2009: Time-dependent changes in extreme-precipitation return-period amounts in the continental United States. *J. Appl. Meteor. Climatol.*, **48**, 2086–2099, https://doi.org/10.1175/2009JAMC2179.1.

——, W. Noon, and K. L. Eggleston, 2015: Efficient access to climate products using ACIS web services. *Bull. Amer. Meteor. Soc.*, **96**, 173–180, https://doi.org/10.1175/BAMS-D-13-00032.1.

Dwyer, J. G., and P. A. O'Gorman, 2017: Changing duration and spatial extent of midlatitude precipitation extremes across different climates. *Geophys. Res. Lett.*, **44**, 5863–5871, https://doi.org/10.1002/2017GL072855.

Easterling, D. R., J. L. Evans, P. Ya. Groisman, T. R. Karl, K. E. Kunkel, and P. Ambenje, 2000: Observed variability and trends in extreme climate events: A brief review. *Bull. Amer. Meteor. Soc.*, **81**, 417–426, https://doi.org/10.1175/1520-0477(2000)081<0417:OVATIE>2.3.CO;2.

ETCCDI, 2013: Expert Team on Climate Change Detection and Indices ETCCDI/CRD climate change indices: Software. Accessed 25 November 2019, http://etccdi.pacificclimate.org/software.shtml.

Groisman, P. Ya., R. W. Knight, and T. R. Karl, 2012: Changes in intense precipitation over the central United States. *J. Hydrometeor.*, **13**, 47–66, https://doi.org/10.1175/JHM-D-11-039.1.

Hayhoe, K., and Coauthors, 2007: Past and future changes in climate and hydrological indicators in the US Northeast. *Climate Dyn.*, **28**, 381–407, https://doi.org/10.1007/s00382-006-0187-8.

Henn, B., A. J. Newman, B. Livneh, C. Daly, and J. D. Lundquist, 2018: An assessment of differences in gridded precipitation datasets in complex terrain. *J. Hydrol.*, **556**, 1205–1219, https://doi.org/10.1016/j.jhydrol.2017.03.008.

Hoerling, M., J. Eischeid, J. Perlwitz, X. W. Quan, K. Wolter, and L. Cheng, 2016: Characterizing recent trends in U.S. heavy precipitation. *J. Climate*, **29**, 2313–2332, https://doi.org/10.1175/JCLI-D-15-0441.1.

Huang, H., J. M. Winter, E. C. Osterberg, R. M. Horton, and B. Beckage, 2017: Total and extreme precipitation changes over the northeastern United States. *J. Hydrometeor.*, **18**, 1783–1798, https://doi.org/10.1175/JHM-D-16-0195.1.

Hunter, R. D., and R. K. Meentemeyer, 2005: Climatologically aided mapping of daily precipitation and temperature. *J. Appl. Meteor.*, **44**, 1501–1510, https://doi.org/10.1175/JAM2295.1.

Keim, B. D., M. R. Fischer, and A. M. Wilson, 2005: Are there spurious precipitation trends in the United States Climate Division database? *Geophys. Res. Lett.*, **32**, L04702, https://doi.org/10.1029/2004GL021985.

Knapp, K. R., 2008: Scientific data stewardship of International Satellite Cloud Climatology Project B1 global geostationary observations. *J. Appl. Remote Sens.*, **2**, 023548, https://doi.org/10.1117/1.3043461.

Kunkel, K. E., D. R. Easterling, D. A. R. Kristovich, B. Gleason, L. Stoecker, and R. Smith, 2012: Meteorological causes of the secular variations in observed extreme precipitation events for the conterminous United States. *J. Hydrometeor.*, **13**, 1131–1141, https://doi.org/10.1175/JHM-D-11-0108.1.

——, and Coauthors, 2013a: Monitoring and understanding trends in extreme storms: State of knowledge. *Bull. Amer. Meteor. Soc.*, **94**, 499–514, https://doi.org/10.1175/BAMS-D-11-00262.1.

——, and Coauthors, 2013b: Regional climate trends and scenarios for the U.S. National Climate Assessment: Part 1—Climate of the Northeast U.S. NOAA Tech. Rep. NESDIS 142-1, 80 pp., https://www.nesdis.noaa.gov/sites/default/files/asset/document/NOAA_NESDIS_Tech_Report_142-1-Climate_of_the_Northeast_US.pdf.

Lai, Y., and D. A. Dzombak, 2019: Use of historical data to assess regional climate change. *J. Climate*, **32**, 4299–4320, https://doi.org/10.1175/JCLI-D-18-0630.1.

Le, P. D., A. C. Davison, S. Engelke, M. Leonard, and S. Westra, 2018: Dependence properties of spatial rainfall extremes and areal reduction factors. *J. Hydrol.*, **565**, 711–719, https://doi.org/10.1016/j.jhydrol.2018.08.061.

Livneh, B., E. A. Rosenberg, C. Lin, B. Nijssen, V. Mishra, K. M. Andreadis, E. P. Maurer, and D. P. Lettenmaier, 2013: A long-term hydrologically based dataset of land surface fluxes and states for the conterminous United States: Update and extensions. *J. Climate*, **26**, 9384–9392, https://doi.org/10.1175/JCLI-D-12-00508.1.

——, T. J. Bohn, D. W. Pierce, F. Munoz-Arriola, B. Nijssen, R. Vose, D. R. Cayan, and L. Brekke, 2015: A spatially comprehensive, hydrometeorological data set for Mexico, the U.S., and southern Canada 1950–2013. *Sci. Data*, **2**, 150042, https://doi.org/10.1038/sdata.2015.42.

Mass, C., A. Skalenakis, and M. Warner, 2011: Extreme precipitation over the west coast of North America: Is there a trend? *J. Hydrometeor.*, **12**, 310–318, https://doi.org/10.1175/2010JHM1341.1.

Mauget, S. A., 2006: Intra- to multi-decadal terrestrial precipitation regimes at the end of the 20th century. *Climatic Change*, **78**, 317–340, https://doi.org/10.1007/s10584-006-9129-z.

Maurer, E. P., A. W. Wood, J. C. Adam, D. P. Lettenmaier, and B. Nijssen, 2002: A long-term hydrologically based dataset of land surface fluxes and states for the conterminous United States. *J. Climate*, **15**, 3237–3251, https://doi.org/10.1175/1520-0442(2002)015<3237:ALTHBD>2.0.CO;2.

Menne, M. J., I. Durre, R. S. Vose, B. E. Gleason, and T. G. Houston, 2012: An overview of the Global Historical Climatology Network-Daily database. *J. Atmos. Oceanic Technol.*, **29**, 897–910, https://doi.org/10.1175/JTECH-D-11-00103.1.

Mesinger, F., and Coauthors, 2006: North American Regional Reanalysis. *Bull. Amer. Meteor. Soc.*, **87**, 343–360, https://doi.org/10.1175/BAMS-87-3-343.

Min, S.-K., X. Zhang, F. W. Zwiers, and G. C. Hegerl, 2011: Human contribution to more-intense precipitation extremes. *Nature*, **470**, 378–381, https://doi.org/10.1038/nature09763.

Nguyen, P., M. Ombadi, S. Sorooshian, K. Hsu, A. AghaKouchak, D. Braithwaite, H. Ashouri, and A. R. Thorstensen, 2018: The PERSIANN family of global satellite precipitation data: A review and evaluation of products. *Hydrol. Earth Syst. Sci.*, **22**, 5801–5816, https://doi.org/10.5194/hess-22-5801-2018.

Ombadi, M., P. Nguyen, S. Sorooshian, and K. L. Hsu, 2018: Developing intensity–duration–frequency (IDF) curves from satellite-based precipitation: Methodology and evaluation. *Water Resour. Res.*, **54**, 7752–7766, https://doi.org/10.1029/2018WR022929.

Peterson, T. C., and Coauthors, 2013: Monitoring and understanding changes in heat waves, cold waves, floods, and droughts in the United States: State of knowledge. *Bull. Amer. Meteor. Soc.*, **94**, 821–834, https://doi.org/10.1175/BAMS-D-12-00066.1.

Prein, A. F., C. Liu, K. Ikeda, S. B. Trier, R. M. Rasmussen, G. J. Holland, and M. P. Clark, 2017: Increased rainfall volume

from future convective storms in the US. *Nat. Climate Change*, **7**, 880–884, https://doi.org/10.1038/s41558-017-0007-7.

PRISM Climate Group, 2016: Descriptions of PRISM spatial climate datasets for the conterminous United States. PRISM Doc., 22 pp., http://www.prism.oregonstate.edu/documents/PRISM_datasets.pdf.

Pryor, S. C., J. A. Howe, and K. E. Kunkel, 2009: How spatially coherent and statistically robust are temporal changes in extreme precipitation in the contiguous USA? *Int. J. Climatol.*, **29**, 31–45, https://doi.org/10.1002/joc.1696.

Rosenzweig, C., W. Solecki, and A. DeGaetano, 2011: ClimAID: Integrated assessment for effective climate change adaptation strategies in New York State. *Ann. N. Y. Acad. Sci.*, **1244**, 1–14.

Shepard, D. S., 1984: Computer mapping: The SYMAP interpolation algorithm. *Spatial Statistics and Models*, G. L. Gaile and C. J. Willmott, Eds., Springer, 133–145.

Sorooshian, S., K.-L. Hsu, X. Gao, H. V. Gupta, B. Imam, and D. Braithwaite, 2000: Evaluation of PERSIANN system satellite-based estimates of tropical rainfall. *Bull. Amer. Meteor. Soc.*, **81**, 2035–2046, https://doi.org/10.1175/1520-0477(2000)081<2035:EOPSSE>2.3.CO;2.

Timmermans, B., M. Wehner, D. Cooley, T. O'Brien, and H. Krishnan, 2019: An evaluation of the consistency of extremes in gridded precipitation data sets. *Climate Dyn.*, **52**, 6651–6670, https://doi.org/10.1007/s00382-018-4537-0.

Trenberth, K. E., L. Cheng, P. Jacobs, Y. Zhang, and J. Fasullo, 2018: Hurricane Harvey links to ocean heat content and climate change adaptation. *Earth's Future*, **6**, 730–744, https://doi.org/10.1029/2018EF000825.

Wasko, C., A. Sharma, and S. Westra, 2016: Reduced spatial extent of extreme storms at higher temperatures. *Geophys. Res. Lett.*, **43**, 4026–4032, https://doi.org/10.1002/2016GL068509.

Widmann, M., and C. S. Bretherton, 2000: Validation of mesoscale precipitation in the NCEP reanalysis using a new gridcell dataset for the northwestern United States. *J. Climate*, **13**, 1936–1950, https://doi.org/10.1175/1520-0442(2000)013<1936:VOMPIT>2.0.CO;2.

Wuebbles, D. J., D. W. Fahey, K. A. Hibbard, D. J. Dokken, B. C. Stewart, and T. K. Maycock, Eds., 2017: *Climate Science Special Report: Fourth National Climate Assessment*. Vol. I. U.S. Global Change Research Program, 470 pp., https://doi.org/10.7930/J0J964J6.